Hot deformation behavior and processing maps of diamond/Cu composites

HONGDI ZHANG, YUE LIU, FAN ZHANG, DI ZHANG, HANXING ZHU and TONGXIANG FAN

Hot deformation behavior of 50 vol.% uncoated and Cr-coated diamond/Cu composites were investigated by hot isothermal compression tests in the temperature range between 1073 K and 1273 K (800 ℃ and 1000 ℃) with strain rate range of 0.001-5 s^{-1}. The results reveal that dynamic recrystallization is the primary restoration mechanism during the deformation. The coating film Cr_7C_3 enhanced the interfacial bonding and resulted in a larger flow stress of Cr-coated diamond/Cu composites. Moreover, the enhanced interface affinity led to a higher activity energy (238 kJ/mol) than that of uncoated diamond/Cu composites (205 kJ/mol). The strain-rate dependent constitutive equations of diamond/Cu composites were derived based on the Arrhenius model and the results indicated a high correlation (R = 0.99) between the calculated flow stresses and the experimental data. With the help of processing maps, hot extrusion was realized at 1123 K/0.01s^{-1} (850 ℃/0.01s^{-1}) and 1153 K/0.01^{-1} (880 ℃/0.01s^{-1}) for uncoated and coated diamond/Cu composites. The combination of interface optimization and hot extrusion brought to the increment of density and thermal conductivity, which provided a promising option to fabricate diamond/Cu composites.

HONGDI ZHANG, FAN ZHANG, DI ZHANG, and TONGXIANG FAN are with the State Key Laboratory for Metal Matrix Composites, School of Materials Science and Engineering, Shanghai Jiao Tong University, Shanghai 200240, China. Contact e-mail: txfan@sjtu.edu.cn HANXING ZHU is with School of Engineering, Cardiff University, Cardiff, CF24 3AA, UK.

I. Introduction

High thermal conductivity materials are widely used in extreme environment with high heat flux and consistent thermocycling [1-3]. In recent years, diamond/Cu composites, which combine diamond with the highest thermal conductivity and low-cost copper, have attracted more and more attention for their high thermal conductivity and thermal stability. However, copper is non-wetting and non-chemical affinity with diamond and easy to result in interfacial debonding. The voids act as high thermal resistance and significantly decrease the thermal conductivity of composites [4]. In order to ameliorate the diamond-copper interface, metal matrix alloying [5, 6] or diamond surface metallization (molten salt method [7-9], magnetron sputtering [10], and vapor deposition [11]) can be utilized. Due to its operability and efficiency, the molten salt method is widely used in diamond surface metallization. Generally, transition element Cr can be used to enhance the interface bonding for the low reaction temperature and reaction production with high thermal conductivity [8]. However, voids still remain in the powder metallurgy sintering (such as spark plasma sintering, SPS) diamond/Cu composites, even with diamond surface metallization [12].

In order to improve the quality and density of composites, plastic deformation processing (extrusion, rolling and forging) can be utilized, which is usually employed in the preparation of composites using powder metallurgy, such as the preparation of TiC_p/AZ91D, SiC_p/2009Al and SiC_w-2124A1 [13-15]. Nevertheless, there have been few studies on the hot deformation of diamond/Cu composites because the presence of diamond severely reduces the workability of composites due to the increase of dislocation density in matrix copper. In addition, most studies are focused on the particles reinforced metal matrix composites (MMCs) with low particle content ($\leq 30\%$) [16]. The high volume fraction ($\geqslant 50\%$) of diamond generates great residual stress in composites, which limits the dislocation slip and leads to deformation instability [17]. Therefore, it is necessary to investigate the influence of reinforcement on the workability of diamond/Cu composites. Generally, constitutive equation and hot processing maps are used to investigate the workability of alloys and composites. The hot deformation behavior can be fully understood through constitutive equation, which

is proposed by Sellars and Tegart through introducing the correlation between strain and stress [18]. The hot processing maps, which are based on dynamic materials model (DMM), directly display the favorable hot deformation strain rates and temperatures.

In this study, we performed a comparative study of hot deformation behavior of diamond/Cu composites. The diamond surface metallization was conducted using the molten salt method. A series of isothermal compression tests were conducted in the temperature range between 1073 K and 1273 K (800 ℃ and 1000 ℃) with strain rate range of 0.001-5 s^{-1} for uncoated and Cr-coated diamond/Cu composites. The constitution equations were established on the basis of Arrhenius model and the derived flow stresses were in good agreement with the experimental data. Hot extrusion of 50 vol.% diamond/Cu composites were realized with the help of processing maps, which were established under the dynamic materials modeling (DMM) and instability criteria. In order to evaluate the effect of hot extrusion, the microstructure and thermal conductivity were characterized.

II. Experimental

A. *Raw materials and pretreatment*

The reinforcement diamonds (135 μm) were provided by Henan Huanghe Whirlwind Co., China. The diamond surface metallization reagent of chromium (99% purity, 40 μm) was provided by Sigma-Aldrich Co. Analytical grade NaCl and KCl were provided by Sinopharm Chemical Regent Co., LTD, China. The copper powder (99% purity, 20 μm) was provided by Sigma-Aldrich Co.

Raw diamond and chromium were mixed with molar ratio of 10:1 and the mixture was subsequently covered with chloride salts (molar ratio of KCl: NaCl=1:1). The diamond surface metallization was carried out at 1173 K (900 ℃) for 60 minutes. The metallization was processed in a tube furnace under high purity argon and the coated diamond particles were washed three times with boiling deionized water under ultrasonic.

B. *SPS, hot compression tests and hot extrusion*

The uncoated and coated diamond particles were mixed with copper powder in

planetary ball mill for 12 hours under vacuum, respectively (For the ultra-high hardness of diamond, the mixing was proceeded without stain balls). The spark plasma sintering (SPS) system was used to fabricate the 50 vol.% uncoated and coated diamond/Cu composites at 1193 K (920 ℃) with a holding time of 10 minutes in a graphite die. The heating rate was 100 K/min and the pressure was 50 MPa.

The hot compression tests were conducted using the Gleeble-3500 test system between 1073 K to 1273 K (800 ℃ and 1000 ℃) with 50 K intervals at strain rates of 0.001, 0.01, 0.1, 1, and 5 s^{-1} to strain of $\varepsilon = 0.4$. Due to the hard machining, the uncoated and coated diamond/Cu composites were cut by laser into cylinders with size of 8 mm in diameter and 12 mm in height. All of the samples were polished with diamond abrasive to reduce the surface flaw and the ends of the specimen were lubricated with graphite lubricant. The temperature was maintained for 5 minutes after the test temperature was achieved and the samples were water quenched after tests.

In order to promote the extrusion die release, half extrusion die was used. The sintering samples and extrusion die were brushed with graphite lubricant. The stainless steel extrusion cylinder and extrusion die were heated to 773 K (500 ℃) before hot extrusion was performed. The uncoated and coated diamond/Cu composites were maintained at 1123 K and 1153 K (850 ℃ and 880 ℃) for 5 minutes, respectively. The hot extrusion was carried out at 0.01 s^{-1} strain rate with an extrusion ratio of 10:1, after which the extruded rods were cooled down to room temperature.

C. *Materials characterization*

The phase structure of the raw diamond and Cr-coated diamond were characterized by X-ray diffraction (XRD, Ultima IV, Rigaku), using Cu Kα (λ = 1.5406 Å) radiation at 35 kV and 200 mA. The data was collected in the range of 10-130º (2θ) with a step of 0.02º and a scan rate of 5º/min.

In order to achieve high quality surface finishing, the extruded samples were manufactured using the Leica EMTIC3X TIB slope cutter. The surface morphology of raw diamond, coated diamond, and cross sections of uncoated and coated diamond/Cu composites were characterized using a field emission scanning electron microscopy (SEM, FEI NOVA NanoSEM 230). The interface microstructure and energy dispersive

spectrometer (EDS) characterization were also performed using the field emission SEM. The thermal conductivity of diamond/Cu composites was measured using the laser flash method and the thermal conductivity was calculated through

$$k = \alpha \cdot \rho \cdot C_p \quad (1)$$

where k is thermal conductivity, α is thermal diffusivity, ρ is bulk density of samples, and C_p is specific heat. The thermal diffusivity α was measured using a Netzsch LFA 447 Laser Flash Apparatus and samples of 10 mm in diameter and 3 mm in thickness. The density was determined using a densitometer and the specific heat of diamond/Cu composites was measured using a differential scanning calorimeter.

II. Results and discussion

A. *Diamond Surface Metallization*

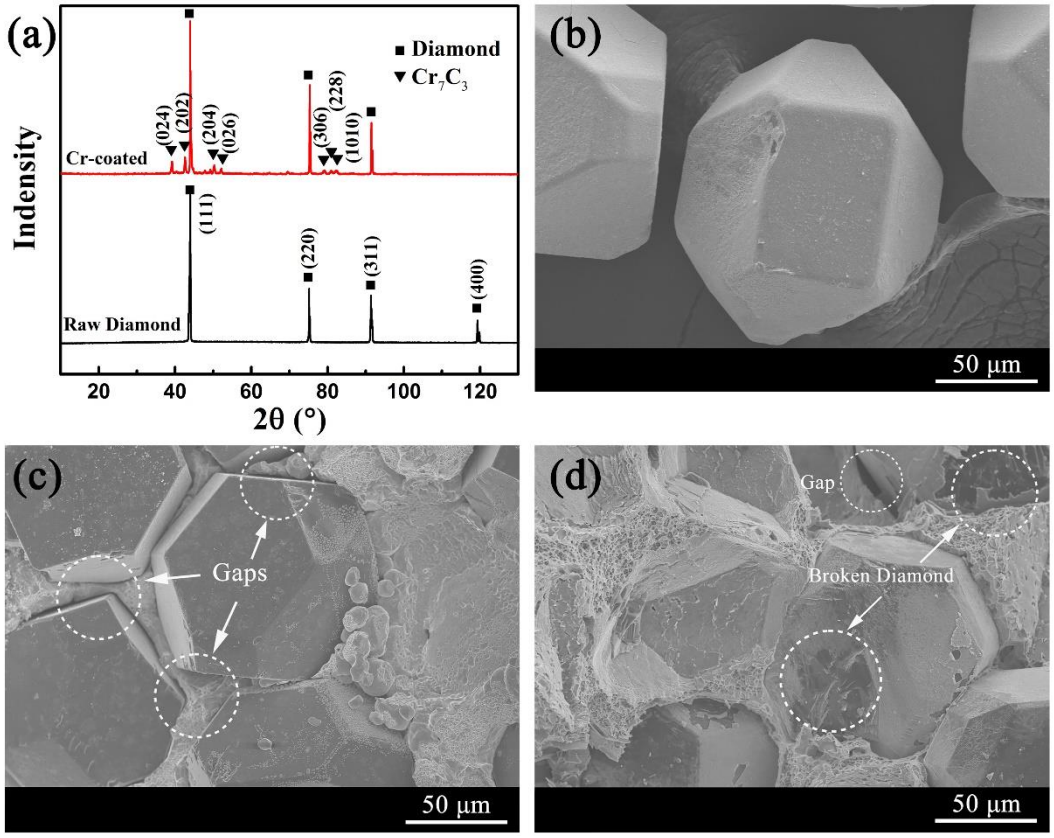

Fig. 1—(a) XRD patterns of raw diamond and diamond coated at 1173 K (900 ℃) for 60 minutes; (b) SEM images of Cr-coated diamond; Fracture surface SEM images of 50 vol.% (c) uncoated and (d) coated diamond/Cu composites.

Figure 1a presents the XRD patterns of raw diamond and surface metallized diamond at 1173 K (900 ℃) for 60 minutes. The reaction production is identified as Cr_7C_3, which is in good agreement with other studies [8, 19]. As can be seen in Figure 1b, the diamond particles were fully covered. Figure 1c shows the fracture surface microstructure of sintering 50 vol.% uncoated diamond/Cu composites. A large number of gaps exist between the uncoated diamond and copper, which are due to the non-chemical affinity between copper and carbon [4]. For the coated diamond/Cu composites shown in Figure 1d, the coating film acted as a transition layer and enhanced the interfacial bonding. Moreover, a large number of broken diamond particles were observed in the fracture cross section. Transcrystalline fracture only occurred when the interfacial cohesion strength exceeded the diamond fracture strength [20]. The coating film effectively facilitated the interfacial adhesion between diamond and copper. However, as shown in Figure 1d, minor gaps still existed between coated diamond and cooper. The maximum strength of sintering graphite mold was 50 MPa, which is unable to ensure a sufficient density of 50 vol.% coated diamond and copper composites. Therefore, hot deformation was used to further increase the final density of the composites.

B. *Flow Curves*

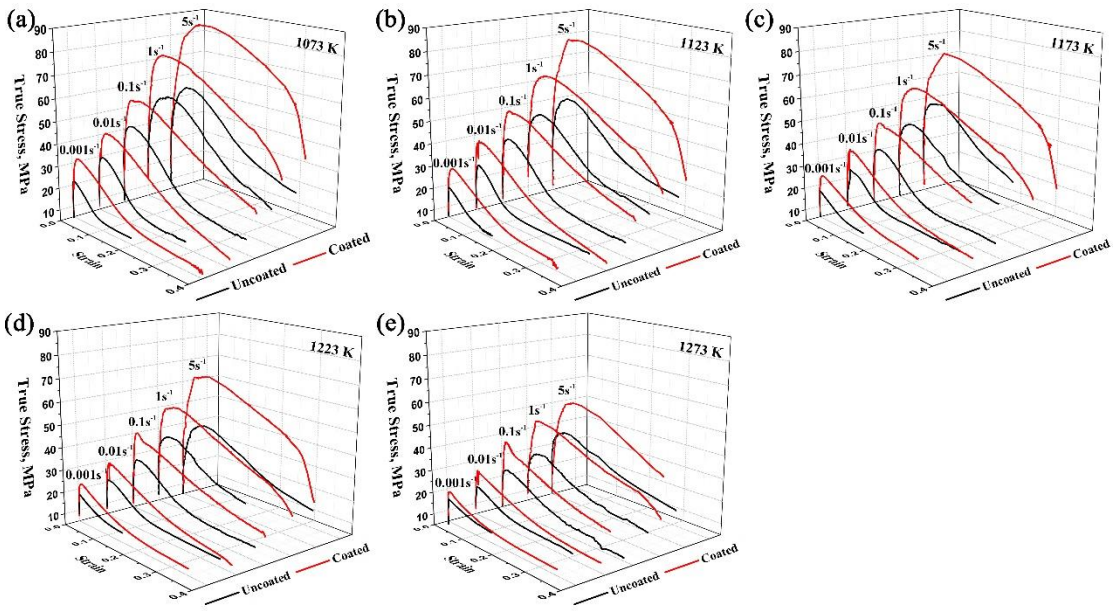

Fig. 2—True stress-strain for 50vol. % uncoated and coated diamond/Cu composites at (a) 1073

K (800 ℃), (b) 1123 K (850 ℃), (c) 1173 K (900 ℃), (d) 1223 K (950 ℃), and (e) 1273 K (1000 ℃) with different strain rates.

Figure 2 shows the true strain-stress curves in the temperature range between 1073 K and 1273 K (800 ℃ and 1000 ℃) with 50 K (50 ℃) intervals at different strain rates of 50 vol.% uncoated and coated diamond/Cu composites. The flow stress (σ) is intimately linked with the deformation temperature (T), strain rate ($\dot{\varepsilon}$), and strain (ε) [13, 16]. During the whole deformation process, work hardening and dynamic softening simultaneously affect the plastic flow. The generation and accumulation of dislocations in matrix resulted in work hardening, while dynamic recrystallization (DRX) and dynamic recovery (DRY) led to dynamic softening [21]. As shown in Figure 2a, the true stress increased sharply with an increase in the strain and reached a peak value at ε = 0.05, which indicates that the work hardening effect was dominant before ε = 0.05, while the stress declined rapidly after the peak value because the dynamic softening effect began to play the dominant role. Youngmoo Kim *et al*. examined the hot deformation behavior of powder sintered oxygen free coppers and found that the DRX was the dominant restoration mechanism [22]. The appearance of peak stress also indicates that characteristic DRX took place during the deformation [18, 23]. The peak stress, as can be seen in Table I, increased with the increase of strain rate from 0.001 to 5 s^{-1} and the highest stress of 57 MPa appeared with $\dot{\varepsilon}$ = 5 s^{-1} at 1073 K (800 ℃). For the coated diamond/Cu composites, the peak stress was higher than that of uncoated diamond/Cu composites. This difference was only 15 MPa at 0.001 s^{-1}, but 24 MPa at 5 s^{-1}. As shown in Figure 2b-2e, the peak stress decreased with the increase of deformation temperature. The improved dislocation movements and DRX softening at high temperatures jointly resulted in a reduced flow stress difference [16].

Table I. Peak stress (in MPa) of uncoated and coated diamond/Cu composites at ε =0.05.

Samples	Temperature (K(℃))	Strain rate (s^{-1})				
		0.001	0.01	0.1	1	5
Uncoated	1073 (800)	15.49	26.92	41.74	54.03	57.07
	1123 (850)	13.34	21.98	35.85	46.78	52.15
	1173 (900)	12.45	22.29	30.47	42.18	49.45
	1223 (950)	12.92	18.71	27.03	37.62	40.81
	1273 (1000)	12.46	15.17	22.14	29.34	37.47
Coated	1073 (800)	30.79	41.77	55.12	73.77	80.81
	1123 (850)	26.26	36.25	49.46	64.37	79.12
	1173 (900)	22.41	31.27	42.71	59.05	69.31
	1223 (950)	19.38	27.16	37.58	51.78	63.31
	1273 (1000)	15.37	22.78	31.69	45.11	51.27

DRX initiates that during the plastic deformation, the critical strain ε_c depends on the temperature and strain rate. As to the diamond/Cu composites system, the occurance of DRX can be determined using work hardening analysis. Poliak and Jonas have used the relationship between ($-\partial\theta/\partial\sigma$) and σ to determine the occurrence of DRX [24]. The strain hardening rate θ was obtained through $\partial\sigma/\partial\varepsilon$ and the initiation of DRX was determined by the differentiation of $-\partial\theta/\partial\sigma$ at the minimum point [25]. As shown in Figure 3a, the DRX starts from σ = 23 MPa at ε_c = 0.005 for the uncoated diamond/Cu composites under deformation at 1123 K/0.01s^{-1} (850 ℃/0.01s^{-1}), while the DRX initiation point was 27 MPa at ε_c = 0.003 for the coated diamond/Cu composites as shown in Figure 3b. The DRX initiation for the coated diamond/Cu composites occurs at a larger flow stress than uncoated diamond/Cu composites, resulting in the larger peak flow stress.

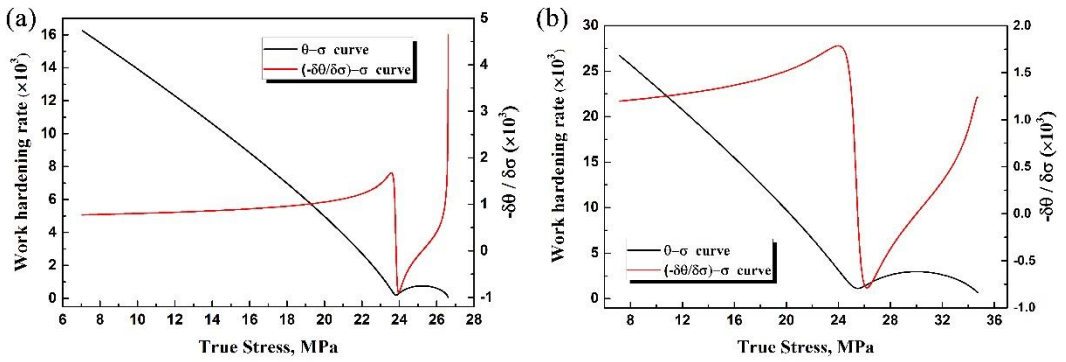

Fig. 3—Flow stress dependence of θ and $(-\partial\theta/\partial\sigma)$ at 1123 K/0.01s^{-1} (850 ℃/0.01s^{-1}) of (a) uncoated and (b) coated diamond/Cu composites.

C. *Constitutive Equation*

For the hot deformation of metallic materials, the flow stress is determined by the thermal activation process, as described by some constitutive equations [26]. The Arrhenius model provides a good approximation for the relationship between the flow stress and the Zener-Hollomon parameter [26, 29], and explicitly elucidates the dependence of the Zener-Hollomon parameter on the flow stress, deformation temperature, strain rate, and strain, as given as

$$Z = A[\sinh(\alpha\sigma)]^n = \dot{\varepsilon}exp(Q/RT) \tag{2}$$

which can also be written as

$$\dot{\varepsilon} = A[\sinh(\alpha\sigma)]^n exp(-Q/RT) \tag{3}$$

where Z is the Zener-Hollomon parameter, A, α, and n are constants independent of temperature, R is universal gas constant (8.314 J/(mol·K)), T is in K, and Q is the apparent activation energy in kJ/mol. Due to the magnitude of the flow stress at different strain rates, Equation (3) can be rewritten in the natural logarithm form, and given as

$$\ln\dot{\varepsilon} = n' \ln\sigma + \ln A_1, \ \alpha\sigma < 0.8 \tag{4}$$

$$\ln\dot{\varepsilon} = \beta\sigma + \ln A_2, \ \alpha\sigma > 1.2 \tag{5}$$

$$\ln\dot{\varepsilon} = n\ln[\sinh(\alpha\sigma)] + \ln A_3 - Q/RT, \text{ for all } \sigma \tag{6}$$

The constants n' and β are the slopes of the fitting lines of $\ln\dot{\varepsilon}$ against lnσ and $\ln\dot{\varepsilon}$ against σ, respectively. The constant α is determined through $\alpha = \beta/n'$. The constant n is obtained as the slope of the fitting line of $\ln\dot{\varepsilon}$ against ln[sinh(ασ)].

The apparent activation energy Q indicates the plastic deformability of a material

at high deformation temperature, which can be expressed as follows:

$$Q = 10000 \cdot R \cdot \left[\frac{\partial \ln \dot{\varepsilon}}{\partial \ln[\sinh(\alpha\sigma)]}\right]_T \cdot \left[\frac{\partial \ln[\sinh(\alpha\sigma)]}{\partial(10000/T)}\right]_{\dot{\varepsilon}} \quad (7)$$

The value of A_3 is determined as the intercept of the fitting line of ln$Z$ against ln[sinh(ασ)] from the natural logarithm of equation (2), and given as

$$\ln Z = \ln A_3 + n \ln[\sinh(\alpha\sigma)] \quad (8)$$

With the material constants (n', β, α, n, Q) in the constitutive equation, the flow stress can be obtained as

$$\sigma = \frac{1}{\alpha} ln\left\{(Z/A)^{1/n} + \left[(Z/A)^{2/n} + 1\right]^{1/2}\right\} \quad (9)$$

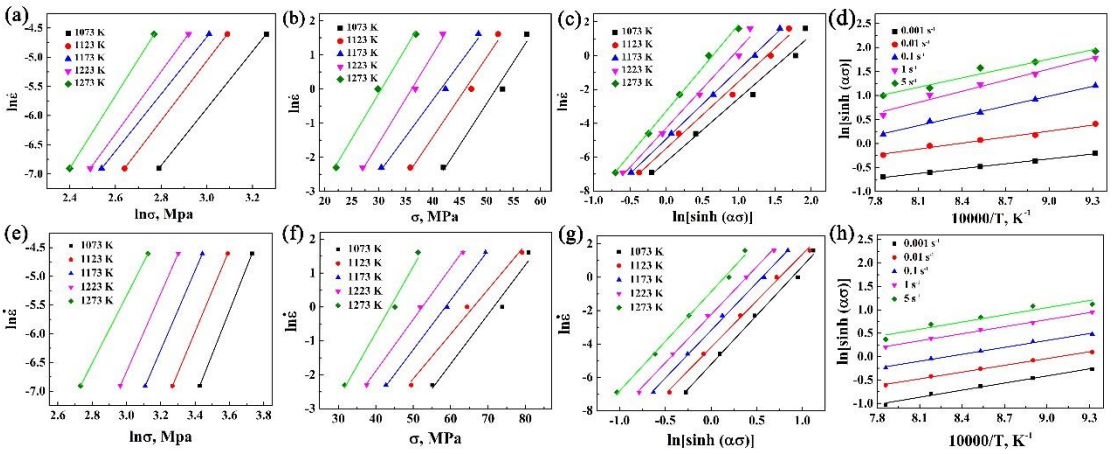

Fig. 4—Plots of (a) and (e) $\ln\dot{\varepsilon}$ vs ln σ; (b) and (f) $\ln\dot{\varepsilon}$ vs σ; (c) and (g) $\ln\dot{\varepsilon}$ vs ln[sinh (ασ)]; (d) and (h) 10000/T vs ln[sinh (ασ)] for constitutive equation calculations. (a)-(d), (e)-(h) are calculations of uncoated and coated diamond/Cu composites, respectively.

Figure 4 shows the calculation of constitutive equations for uncoated and coated diamond/Cu composites at ε = 0.05 and the materials constants in the constitutive equations are listed in Table II. As shown in Figure 4a and 4e, the material constant n' was determined through the slope of fitting line at low strain rates ($\dot{\varepsilon} =$ 0.001 and 0.01 s^{-1}). As to the flow curves with high strain rates ($\dot{\varepsilon} =$ 0.1, 1, 5 s^{-1}), the constant β was obtained through the fitting line in Figure 4b and 4f. Therefore, the constant α can be determined as 0.046 and 0.023 for the uncoated and coated diamond/Cu composites, respectively. Equation (6) displays the relationship between $\ln\dot{\varepsilon}$ and ln [sinh ($\alpha\sigma$)] at all stain rates, hence, the constant n was obtained by the fitting line in Figure 4c and 4g.

Table II. Constants in the constitutive equation of uncoated and coated diamond/Cu composites deformed at $\varepsilon = 0.05$.

Materials	n'	β	α	n	Q (kJ/mol)
Uncoated diamond/Cu composites	5.299	0.2436	0.046	4.317	205
Coated diamond/Cu composites	6.854	0.1561	0.023	5.782	238

The activation energies Q of diamond/Cu composites can be determined using Equation (7) with the constant n and the slope of fitting line in Figure 4d and 4h, which manifest the relationships between ln [sinh ($\alpha\sigma$)] and 10000/T. The activation energies Q = 205 and 238 kJ/mol for uncoated and coated diamond/Cu composites, respectively. M. Hörnqvist *et al*. studied the deformation and texture evolution of oxygen-free high conductivity copper and obtained the activity energy as 210 kJ/mol for lattice self-diffusion of copper [27]. It noted that the deformation behavior is mainly controlled by the lattice self-diffusion for the uncoated diamond/Cu composites. However, the activation energy increased to 238 kJ/mol for the coated diamond/Cu composites. This is attributed to the increase of interfacial affinity between matrix copper and reinforcement diamond particles. For low stacking fault energy metal, such as copper, the deformation was determined by dislocation aggregation, climb and cross-slip [16]. As for the reinforcement diamond particles bonded tightly with matrix copper, the movement of dislocations and boundaries is pinned and it leads to a further increase of activation energy [28, 29].

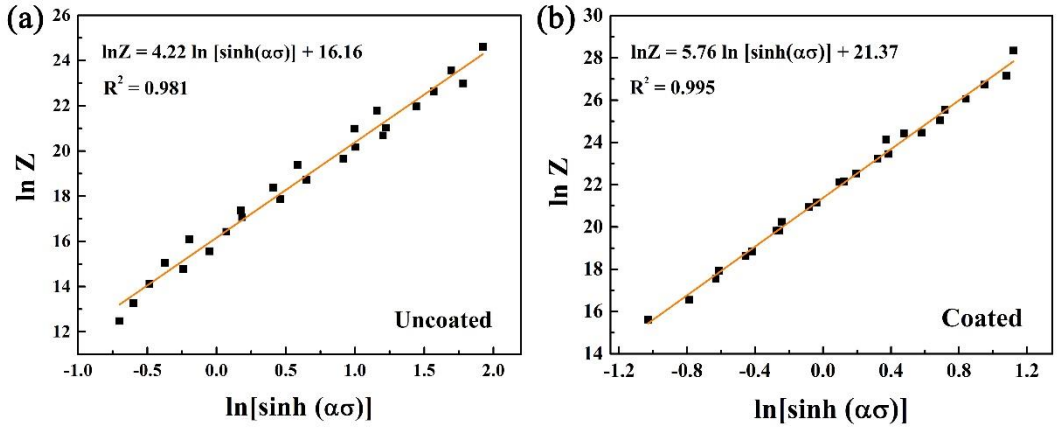

Fig. 5—Relationships between ln$Z$ and ln [sinh(ασ)] of (a) uncoated and (b) coated diamond/Cu composites at ε = 0.05.

Figure 5 shows the relationships between the Zener-Hollomon parameter and the flow stress and both the plots of lnZ against ln[sinh(ασ)] present a linear relationship. The correlation coefficients of the fitting lines were very close to 1 (R^2 = 0.981 and R^2 = 0995 for uncoated and coated diamond/Cu composites, respectively). Based on the above calculations, the constitutive equation for 50 vol.% uncoated diamond/Cu composites at ε = 0.05 can be written as follows:

$$\sigma_{0.05} = \frac{1}{0.046} ln\left\{\left(\frac{Z}{1.04\times10^{7}}\right)^{1/4.317} + \left[\left(\frac{Z}{1.04\times10^{7}}\right)^{2/4.317} + 1\right]^{1/2}\right\} \quad (10)$$

$$\text{where } Z = \dot{\varepsilon}\exp(\frac{205061}{RT}) \quad (11)$$

And for the 50 vol.% coated diamond/Cu composites, it is

$$\sigma'_{0.05} = \frac{1}{0.023} ln\left\{\left(\frac{Z'}{1.93\times10^{9}}\right)^{1/5.782} + \left[\left(\frac{Z'}{1.93\times10^{9}}\right)^{2/5.782} + 1\right]^{1/2}\right\} \quad (12)$$

$$\text{where } Z' = \dot{\varepsilon}\exp(\frac{238436}{RT}) \quad (13)$$

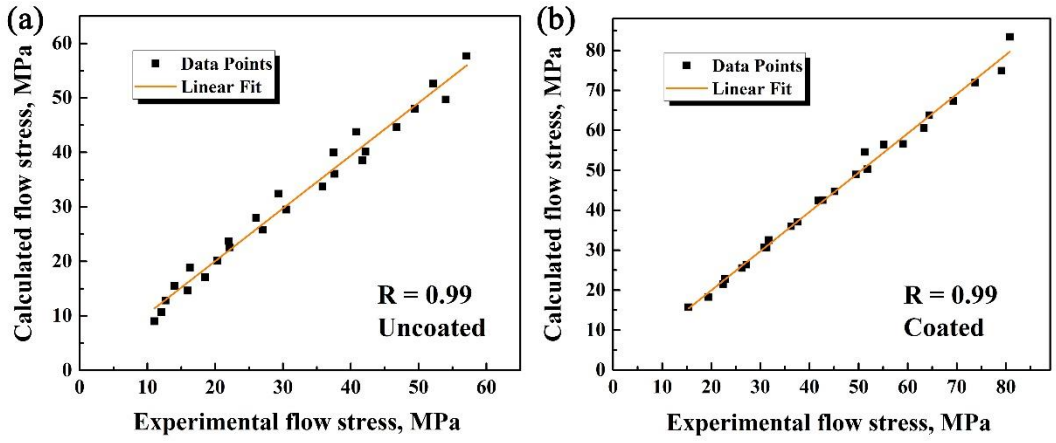

Fig. 6—Comparison between the calculated value and experimental flow stress at ε = 0.05.

In order to verify the accuracy of the above constitutive equations, Figure 6 gives the comparison between the calculated value and experimental flow stress. It can be concluded that a good correlation (R = 0.99) exists between the measured and calculated data for both uncoated and coated diamond copper composites. This

indicates that the established constitutive equations are highly accurate.

D. *Hot Processing Map*

In the hot deformation of materials, processing map is usually used to determine the optimal processing parameters. The hot processing map is established from the efficiency of power dissipation contour based on DMM and the instability map based on stability criteria calculation [30, 31]. During the hot compression deformation, the total input power P is converted into temperature increment of work piece G and dissipation of metallurgical process J. Generally, the metallurgy dissipation J variations represent dynamic material behavior in the hot deformation process. The total input power can be expressed as follows:

$$P = G + J = \int_0^{\sigma} \dot{\varepsilon} d\sigma + \int_0^{\dot{\varepsilon}} \sigma d\dot{\varepsilon} \tag{14}$$

The strain rate sensitivity (m) can be described as the ratio between G and J:

$$\frac{\partial J}{\partial G} = \frac{\dot{\varepsilon}}{\sigma}\frac{\partial \sigma}{\partial \dot{\varepsilon}} = \frac{\partial(\ln\sigma)}{\partial(\ln\dot{\varepsilon})} = m \tag{15}$$

The strain-rate sensitivity m =1 results in the maximum $J_{max} = \sigma\dot{\varepsilon}/2 = P/2$ when the work piece becomes a linear dissipater. In order to reveal the plastic flow of materials, the term of efficiency of power dissipation (η) was introduced as

$$\eta = \frac{J}{J_{max}} = \frac{2m}{m+1} \tag{16}$$

During the hot processing of metals, alloys, or composites, the metallurgical process of DRY and DRX will increase the value of J. The most appreciated processing conditions often give the highest η, which indicate the degree of power dissipation during microstructure evolution [30]. As for the instable deformation, which should be avoided during the hot processing, the flow instability can be calculated by the instability criteria [32]:

$$\xi(\dot{\varepsilon}) = \frac{\partial \ln[m/(m+1)]}{\partial(ln\dot{\varepsilon})} + m < 0 \tag{17}$$

where the $\xi(\dot{\varepsilon})$ is instability parameter.

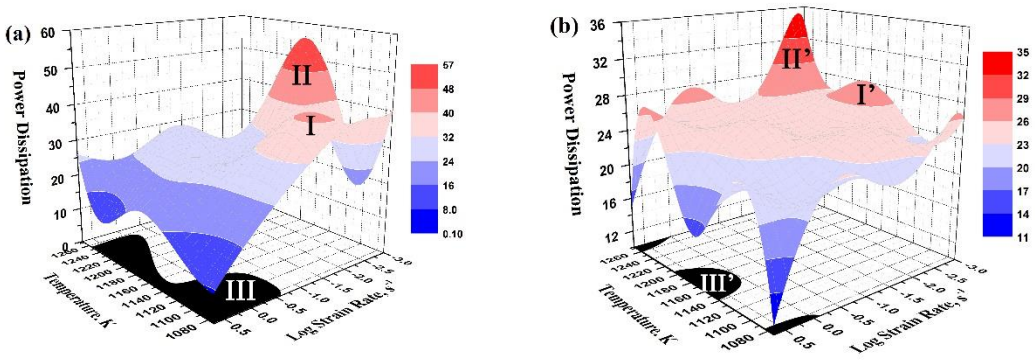

Fig. 7—Processing map for 50 vol. % (a) uncoated and (b) coated diamond/Cu composites at ε=0.05.

Figure 7 shows the processing map of 50 vol.% uncoated and coated diamond/Cu composites at ε = 0.05. The three-dimensional colour contour maps represent the efficiency of power dissipation (η) distribution and the two-dimensional black regions represent instable domains, *i.e.* $\xi(\dot{\varepsilon})$<0. For the uncoated diamond/Cu composites, as shown in Figure 7a, there are two safe processing domains (I and II) and one instable domain (III). The specific ranges are given in Table III. The values of the power dissipation of safe processing domains I and II are both higher than 40%. Youngmoo Kim *et al*. noted that the DRX domains of P/M OFC were within the temperature range of 873 K-1073 K (800 ℃-1000 ℃) and strain rate range of 0.01-1.0 s^{-1}, which are the same as those of the safe processing domain I in this study [33]. As for the domain II, the η was as high as 57%, which can be interpreted as fracturing of diamond particles in the local aggregation. The debonding between uncoated diamond and copper resulted in a large number of voids and aggregation of diamond particles during deformation at high temperature. Therefore, the parameter in region I ($\eta \geqslant 40\%$) can be used for the hot extrusion of uncoated diamond/Cu composites. The high strain rate of instable region III ranging from 0.2 to 5 s^{-1} often resulted in the fracturing of diamond particles, which should be avoided during the hot deformation.

In comparison, as shown in Figure 7b, there are two safe processing domains (I′and II′) and three instable domains (labeled as III′) for the coated diamond/Cu composites. For region II′, the deformation temperature was closed to the melting point of matrix copper, which easily leads to flow instable during the hot deformation. In addition, the

high temperature might result in the damage of diamond particles. Hence, the parameter in region I′ can be utilized for hot extrusion of coated diamond/Cu composites. The high strain rate ($\dot{\varepsilon} \geq 1s^{-1}$) of instable region III′ could result in flow instability, which should be avoided during hot extrusion.

Table III. Temperature range and strain rate range of safe processing domains and instable domains of uncoated and coated diamond/Cu composites.

Uncoated	T (K(℃))	$\dot{\varepsilon}$ (s^{-1})	Coated	T (K(℃))	$\dot{\varepsilon}$ (s^{-1})
I	1083-1123 (810-850)	0.01-0.1	I′	1150-1220 (877-947)	0.001-0.005
II	1138-1208 (865-935)	0.001-0.01	II′	1230-1273 (957-1000)	0.001-0.2
				1073-1083 (800-810)	0.8-5
III	1073-1258 (800-985)	0.2-5	III′	1140-1200 (867-927)	1-5
				1250-1273 (977-1000)	1.1-5

The pictures of uncoated (I and III) and coated (I′, III′) diamond/Cu composites samples after hot compression tests were given in Figure 8. The compressed samples with parameters in safe processing domains I and I′ remained intact, while there were cracks in the sides of samples with instable processing parameters of III and III′. Based on the above discussion, samples with high deformability can be obtained and the instable processing parameters should be avoided in the hot deformation.

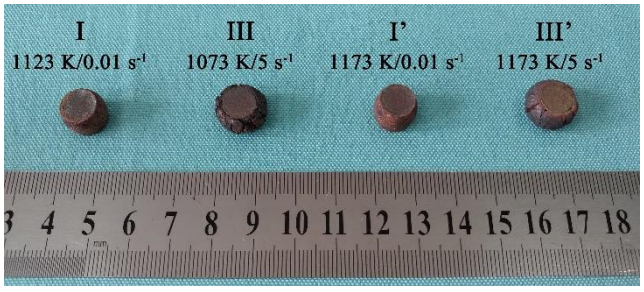

Fig. 8—Actual images of hot compressed samples of uncoated and coated diamond/Cu composites.

E. *Properties and Microstructure*

In order to illustrate the effect of hot extrusion, the microstructure characterization of extruded uncoated and Cr-coated diamond/Cu composites was conducted. Figure 9a shows that the uncoated diamond particles remained intact after the extrusion with the safe processing region I parameters. However, gaps were still observed (labeled with white dotted rectangle) between uncoated diamond particle and matrix copper, even after the hot extrusion. For the extruded Cr-coated diamond/Cu composites with safe processing region I′ parameters, as shown in Figure 9d, the diamond particles sticked closely to the matrix copper and remained intact after hot extrusion. Figure 9e shows that the continuous thin coating film of Cr_7C_3 was distributed around the diamond particles and there were not apparent defects in the interface, which means the interfacial bonding was further ameliorated after extrusion.

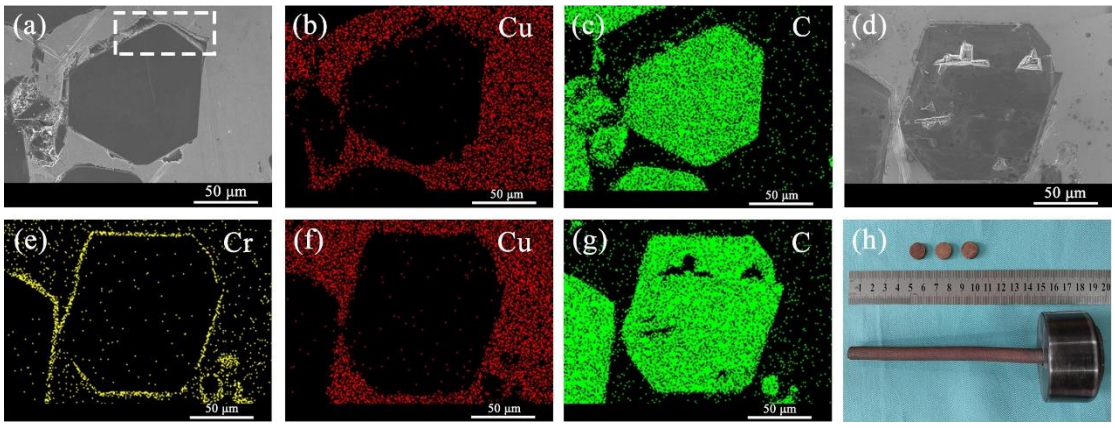

Fig. 9 — SEM images: (a) polished surface of extruded 50 vol.% uncoated diamond/Cu composites; (b) and (c) elemental Cu and C mapping of the SEM image in (a), respectively; (d) polished surface of extruded 50 vol.% Cr-coated diamond/Cu composites; (e-g) elemental mapping of Cr, Cu, and C, respectively. (h) is extruded sample and samples for thermal conductivity tests.

Table IV lists the basic parameters of uncoated, Cr-coated and extruded composites. The thermal conductivity of 50 vol.% uncoated diamond/Cu composites was only 154 W/mk, while it was a little improved after extrusion. However, the thermal conductivity was still much less than the matrix copper, which can be interpreted by the interfacial

debonding between copper and diamond, as shown in Figure 1c. For the coated diamond/Cu composites, the thermal conductivity increased to 413 W/mK for the enhanced interfacial bonding. In contrast, the density of the extruded Cr-coated diamond/Cu composites was further increased and thermal conductivity reached 487 W/mK. The microstructure characterization and thermal conductivity both revealed that the interfacial bonding was ameliorated using the methods of diamond surface metallization and hot extrusion.

Table IV. Thermal conductivity of uncoated, coated and hot extrusion coated diamond/Cu composites.

Samples	Diamond fraction (vol.%)	Density (g/cm^3)	Specific heat (J/gK)	Thermal diffusivity (mm^2/s)	Thermal conductivity (W/mK)
Uncoated	50	6.05	0.405	63	154
Hot extrusion uncoated	50	6.07	0.405	70	172
Coated	50	6.12	0.411	164	413
Hot extrusion coated	50	6.20	0.411	191	487

From the above discussion, it is convinced that the interfacial bonding was ameliorated by the combination of diamond surface metallization and hot deformation, which resulted in the increase of thermal conductivity of diamond copper composites. Future investigation will focus on the precise control of interface thickness.

IV. Conclusions

In this work, the hot deformation behavior of 50 vol.% diamond/Cu composites were investigated using hot compression tests, constitutive equations and hot

processing maps. The hot compression tests were conducted at the temperature range from 1073 K to 1273 K (800 ℃ to 1000 ℃) with 50 K (50 ℃) intervals and at strain rate 0.001-5s^{-1}. During hot deformation, the dominant restoration mechanism of DRX led to dynamic softening. The experimental flow stresses of diamond/Cu composites at $\varepsilon = 0.05$ were consistent with the calculated values from constitutive equations. Due to the introduction of high content of diamond particles and interface amelioration, the movement of the dislocations and boundaries was restricted and the activation energy of coated diamond/Cu composites was increased to 238 kJ/mol. With the help of hot processing map, hot extrusion was realized at 1123 K/0.01 s^{-1} (850 ℃/0.01 s^{-1}) and 1153 K/0.01 s^{-1} (880 ℃/0.01 s^{-1}) for 50 vol.% uncoated and coated diamond/Cu composites, respectively. The thermal conductivity of extruded Cr-coated diamond/Cu composites was increased to 487 W/mK with the improved interfacial bonding.

Acknowledgements

We acknowledge the financial supports of National Key R & D Plan (No.2017YFB0703101) and National Science Fund for Distinguished Young Scholars (No.51425203).

References

1. A.L. Moore and L. Shi: *Mater. Today,* 2014, vol. 17, pp. 163-74.
2. J. Cho and K.E. Goodson: *Nature Mater.,* 2015, vol. 14, pp. 136-37.
3. S. Mallik, N. Ekere, C. Best and R. Bhatti: *Appl. Therm. Eng.,* 2011, vol. 31, pp. 355-62.
4. Christian Monachon and Ludger Weber: *Acta Mater.,* 2014, vol. 73, pp. 337-46.
5. T. Schubert, Ł. Ciupiński, W. Zieliński, A. Michalski, T. Weißgärber and B. Kieback: *Scripta Mater.,* 2008, vol. 58, pp. 263-66.
6. J.W. Li, X.T. Wang, Y. Qiao, Y. Zhang, Z.B. He and H.L. Zhang: *Scripta Mater.,* 2015, vol. 109, pp. 72-75.
7. Y. Zhang, H.L. Zhang, J.H. Wu and X.T. Wang: *Scripta Mater.,* 2011, vol. 65, pp. 1097-100.
8. Q.P. Kang, X.B. He, S.B. Ren, L. Zhang, M. Wu, C.Y. Guo, W. Cui and X.H. Qu: *Appl. Therm. Eng.,* 2013, vol. 60, pp. 423-29.
9. J.M. Molina-Jordá: *Acta Mater.,* 2015, vol. 96, pp. 101-10.
10. W.L. Yang, L.P. Zhou, K. Peng, J.J. Zhu and L. Wan: *Compos. B,* 2013, vol. 55, pp. 1-4.
11. S.B. Ren, X.Y. Shen, C.Y. Guo, N. Liu, J.B. Zang, X.B. He and X.H. Qu: *Compos. Sci. Technol.,* 2011, vol. 71, pp. 1550-55.
12. K. Chu, Z.F. Liu, C.C. Jia, H. Chen, X.B. Liang, W.J. Gao, W.H. Tian and H. Guo: *J. Alloy. Compd.,* 2010,

vol. 490, pp. 453-58.
13. R. Liu, W. Cao, T.X. Fan, C.F. Zhang and D. Zhang: *Mater. Sci. Eng. A,* 2010, vol. 527, pp. 4687-93.
14. Peng Jin, Bolu Xiao, Quanzhao Wang, Zongyi Ma, Yue Liu and Shu Li: *J. Mater. Sci. Technol.,* 2011, vol. 27, pp. 518-24.
15. Soon H. Hong, Kyung H. Chung and Chi H. Lee: *Mater. Sci. Eng. A,* 1996, vol. 206, pp. 225-32.
16. Yu-Li Li, Wen-Xian Wang, Jun Zhou and Hong-Sheng Chen: *Mater. Charact.,* 2017, vol. 124, pp. 107-16.
17. M. Rajamuthamilselvan and S. Ramanathan: *J. Mater. Eng. Perform.,* 2011, vol. 21, pp. 191-96.
18. C.M. Sellars and W.J. Mctegart: *Acta Matall.,* 1966, vol. 14, pp. 1136-38.
19. C. Zhao and J. Wang: *Mater. Sci. Eng. A,* 2013, vol. 588, pp. 221-27.
20. X.Y. Shen, X.B. He, S.B. Ren, H.M. Zhang and X.H. Qu: *J. Alloy. Compd.,* 2012, vol. 529, pp. 134-39.
21. B. K. Raghunath, K. Raghukandan, R. Karthikeyan, K. Palanikumar, U. T. S. Pillai and R. Ashok Gandhi: *J. Alloy. Compd.,* 2011, vol. 509, pp. 4992-98.
22. Y. Kim, S.H. Lee, S. Lee and J.W. Noh: *Mater. Sci. Eng. A,* 2012, vol. 552, pp. 276-82.
23. J.Q. Zhang, H.S. Di, X.Y. Wang, Y. Cao, J.C. Zhang and T.J. Ma: *Mater. Design,* 2013, vol. 44, pp. 354-64.
24. E. I. Poliak and J. J. Jonas: *Acta Mater.,* 1996, vol. 44, pp. 127-36.
25. J.Q. Zhang, H.S. Di, K. Mao, X.Y. Wang, Z.J. Han and T.J. Ma: *Mater. Sci. Eng. A,* 2013, vol. 587, pp. 110-22.
26. John J. Jonas, Xavier Quelennec, Lan Jiang and Étienne Martin: *Acta Mater.,* 2009, vol. 57, pp. 2748-56.
27. M. Hörnqvist, N. Mortazavi, M. Halvarsson, A. Ruggiero, G. Iannitti and N. Bonora: *Acta Mater.,* 2015, vol. 89, pp. 163-80.
28. R. S. Mishra, T. R. Bieler and A. K. Mukherjee: *Acta Metall. Mater.,* 1995, vol. 43, pp. 877-91.
29. Y. Li and T. G. Langdon: *Acta Mater.,* 1998, vol. 46, pp. 3937-48.
30. Y.V.R.K. Prasad, H.L. Gegel, S.M. Doraivelu, J.C. Malas, J.T. Morgan, K.A. Lark and D.R. Barker: *Metall. Mater. Trans. A,* 1984, vol. 15A, pp. 1883-92.
31. Y.V.R.K. Prasad, K.P. Rao and S. Sasidhara: *Hot working guide: A compendium of processing maps*. ASM International, Materials Park, Ohio, 1997.
32. O. Sivakesavam and Y.V.R.K. Prasad: *Mater. Sci. Eng. A,* 2002, vol. A323, pp. 270-77.
33. F.R.N. Nabarro: *Acta Matall.,* 1989, vol. 37, pp. 1521-46.